HHS Public Access

Author manuscript

J Immunol. Author manuscript; available in PMC 2018 August 01.

Published in final edited form as:

J Immunol. 2017 August 01; 199(3): 1003–1011. doi:10.4049/jimmunol.1700256.

Immune cell dynamics in rhesus macaques infected with a Brazilian strain of Zika virus

Eduardo L. V. Silveira[1], **Kenneth A. Rogers**[2], **Sanjeev Gumber**[3], **Praveen Amancha**[2], **Peng Xiao**[2], **Shawna M. Woollard**[4], **Siddappa N. Byrareddy**[4], **Mauro Martins Teixeira**[5], and **Francois Villinger**[2,*]

[1]Department of Clinical and Toxicological Analyses, School of Pharmaceutical Sciences, University of São Paulo, São Paulo-SP, Brazil

[2]New Iberia Research Center, University of Louisiana at Lafayette, New Iberia-LA, USA

[3]Division of Pathology, Yerkes National Primate Research Center, Emory University, Atlanta-GA, USA

[4]Department of Pharmacology and Experimental Neuroscience, University of Nebraska Medical Center, Omaha-NE, USA

[5]Departamento de Microbiologia, Instituto de Ciencias Biologicas, Universidade Federal de Minas Gerais, Belo Horizonte-MG, Brazil

Abstract

Zika virus (ZIKV) is a mosquito-borne and sexually transmitted flavivirus, associated with fetal CNS-damaging malformations during pregnancy in humans. This study documents the viral kinetics, and immune responses in rhesus macaques infected with a clinical ZIKV Brazilian isolate. We evaluated the viral kinetics and immune responses induced after an i.v. infection with a Brazilian ZIKV clinical isolate (HS-2015-BA-01) in rhesus macaques for up to 142 days. ZIKV-specific antibody-secreting cells (ASCs), germinal center (GC) reactions as well as monocyte, DC, NK and T cell frequencies were monitored. ZIKV loads were readily detected in plasma (until day 5 or 7), semen and urine (until day 7 and 14), and saliva (until day 42), but the viremia was rapidly controlled. No detectable clinical manifestations were observed. However, lymph node (LN) hyperplasia was clearly visible post viremia, but associated with low frequencies of ZIKV-specific ASCs in LNs and bone marrow (BM), correlating with low antibody titers. CD14+/CD16- monocytes and myeloid CD11c^{hi} DCs decreased in blood, while NK and T cell numbers were only marginally altered during the course of the study. ZIKV infection caused a significant lymphoid tissue activation but limited induction of ZIKV-specific B cells, suggesting that these parameters need to be considered for ZIKV vaccine design.

Keywords

ZIKV; rhesus macaques; antibody-secreting cells; germinal center reactions; antibody titers; monocytes; dendritic cells; T cells

[*]**Corresponding author**: Dr. Francois Villinger - New Iberia Research Center, University of Louisiana at Lafayette - Address: 4401 W Admiral Doyle Dr, New Iberia - LA, 70560 - USA. Office number: +1(337)482-0225; fjv5939@louisiana.edu.

INTRODUCTION

Zika virus (ZIKV) transmission to humans occurs primarily via mosquito bite, though sexual transmission has been documented (1–3), broadening concerns about the potential of a developing epidemic. The virus was first reported in sentinel rhesus macaques from the Zika forest, Uganda in 1947. A few years later, serologic evidence of ZIKV human infection was detected in several African countries. Due to the few symptomatic cases listed, little clinical importance was given to this infection until the 2007 and 2014 outbreaks in French Polynesia and Brazil respectively (reviewed in (4)).

During those recent ZIKV outbreaks, an increased number of clinical manifestations have been reported, such as microcephaly and arthrogryposis in newborns (5–7) as well as Guillain-Barré syndrome and macula atrophy in adults (8–10). Accurate diagnostics are critical to measure the size of the epidemic and to validate strategies to inhibit viral transmission. Diagnostic kits based on ZIKV-specific monoclonal antibodies have been manufactured, but while positive serology has been an important retrospective diagnostic tool (11), quantitative RT-PCR has been preferably chosen to confirm acute ZIKV infection (12, 13). This strategy has allowed for detection of the viral ability to infect multiple tissues with preferential tropism for myeloid cells (14–16).

Animal models of Zika infection have been established in rodents and nonhuman primates (16–21). Moreover, ZIKV isolates from different locations have been used to characterize animal models and these isolates appear to present distinct patterns of pathogenicity. Recently, it was demonstrated that a ZIKV Brazilian isolate induced significantly higher pathogenicity in neural cells than an African strain (23). Sequencing data revealed that American isolates are more similar to Asian than to African isolates (24). Recent findings in experimental infections of macaque monkeys, show that ZIKV RNA is found in diverse fluids and tissues, but are short-lasting in blood. However, ZIKV loads may last longer in saliva, urine or semen and tissues (16–18, 21, 22). Recently, the extended persistence of ZIKV particles in the testes and epididymidis of IFNar1 KO infected mice was correlated with inflammation, damage of the male genital tract, culminating with lower testosterone levels and infertility (19, 21).

Several experimental ZIKV-specific vaccines and therapeutics have already been developed (25–27)(25–29). Nonetheless, ZIKV-infection elicited immune responses have not been fully described yet. Recent studies showed monocyte and NK cell responses in the first week after infection in macaques as well as ZIKV-specific T cells. Among B cells, total plasmablasts had increased frequency between days 7 and 10 of infection (17, 18). At that time, serum ZIKV NS1-specific IgM and IgG titers were already detected (16, 30).

Thus, in this manuscript we evaluated the unexplored aspects of the innate and adaptive immune responses induced by infection with a primary clinical ZIKV Brazilian isolate in rhesus macaques.

METHODS

Animals and virus challenge

Four male rhesus macaques of Indian origin (A7R078, A7R014, A7L045 and 00-R027) were selected from the breeding colonies of the New Iberia Research Center (NIRC), University of Louisiana at Lafayette (ULL, USA) and housed there for the entire study. Animal ages ranged between 9 (A7R014, A7R078 and A7L045) and 17 (00-R027) years. They were cared for in conformance to the guidelines of the Committee on the Care and Use of Laboratory Animals. All experimental protocols and procedures were reviewed and approved by the ULL Animal Care and Use Committee.

Brazilian ZIKV stocks were provided by Dr. Mauro M. Teixeira, Federal University of Minas Gerais, Brazil, and the challenge strain represented passage number 1 from the clinical sample. C6/36 cells were used to expand that virus and its initial concentration was 1.75×10^9 PFU /mL before challenge. Five $\times 10^7$ PFUs were diluted in 5 mL final volume of PBS and each animal received 1mL via i.v. injection. Peripheral blood mononuclear cells (PBMCs), bone marrow (BM) aspirates and lymph node (LN) and spleen biopsies were obtained at various time points (Figure 1a). Mucosal fluids were collected via Weck-cel collectors as previously described (31).

Viral load determinations

ZIKV viral loads were measured based on ZIKV RNA copies per milliliter of plasma, urine and semen. Total RNA was extracted with QIAamp Viral RNA MiniKit (Qiagen, Valencia, CA). Quantitation of viral RNA was performed using the Taqman RNA-to-Ct 1-Step Kit (Thermo Fisher Scientific, Waltham, MA), according to the manufacturer's protocol on an Applied Biosystems 7500 Real-Time PCR system (Thermo Fisher) using ZIKV-specific primers and probes as previously described (13). Viral loads (copy/ml) were estimated from a standard curve generated using genomic RNA of a Puerto Rican ZIKV strain (PRVABC59 - Centers for Disease Control and Prevention) (BEI resources).

ELISPOT and ELISA

ELISPOT and ELISA were performed as previously described (32)(32). Ninety six well plates were coated with 100 μl of 2.5 μg/mL and 0.5 μg/mL of ZIKV NS1 and domain III of Env (EDIII) proteins (supplied by Luis C. S. Ferreira from The Vaccine Development Laboratory at the University of São Paulo, Brazil) for ELISPOT and ELISA respectively.

Cell staining

Surface and intracellular staining were performed in PBMCs and LN cells as previously described with the following antibodies (clones): Live/Dead (Thermo Fisher); anti-CD3 (SP34-2), anti-CD14 (M5E2), anti-CD123 (7G3), anti-CD80 (L307.4), anti-Ki67 (B56), anti-CD8 (RPA-T8), anti-CD4 (L200), anti-CCR7 (3D12), anti-CD21 (B-Iy4), anti-CD56 (B159), anti-CD95 (DX2), anti-IFNγ (B27) (BD); anti-CD16 (3G8), anti-CD11c (3.9) and anti-PD1 (EH12.2H7) (Biolegend); anti-CD20 (Leu-16) (Becton Dickinson); anti-HLA-DR (Tu36) (Life Technologies); anti-CD19 (CB19) (Abcam); anti-CD38 (AT-1) (Stem Cell Technologies); anti-CADM1 (3E1) (MBL International Corp); anti-CD28 (CD28.2), anti-

NKG2D and anti-NKp44(Z199) (Z231) (Beckman Coulter); anti-CXCR5 (MU5UBEE) (eBioscience); Donkey anti-chicken IgG (polyclonal) (Jackson Immunoresearch Labs); anti-IgD (polyclonal) (Southern Biotech); anti-Perforin (Pf-344) (Mabtech). Samples were acquired on a BD Fusion 14 color cytometer (Mountain View, CA) and analyzed using FlowJo software version 9.9.3 (Tree Star, Ashland, OR).

Immunohistochemistry

Immunofluorescence staining was performed on serial sections for CD20, Ki67, CD3, PD1, CXCR5 and DAPI dye, using a modified protocol previously described (33). Briefly, 4 μm paraffin-embedded tissue sections were subjected to deparaffinization in xylene, rehydration in graded series of ethanol, and rinsing with distilled water. Heat-mediated epitope retrieval was performed with DIVA decloaker, followed by blocking with 10% normal donkey serum (Jackson ImmunoResearch) for 1 hour. Sections were incubated with optimized concentrations of rabbit antihuman-Ki67 (clone SP6, Abcam), mouse antihuman CD20 (clone L26, Dako), Rat anti Human CD3 (clone CD3-12, BIO-RAD), goat polyclonal antihuman PD-1 (AF1086, R& D systems) and rabbit polyclonal anti CXCR5 (HPA042432, Sigma) overnight. Thereafter, the sections were washed and incubated with conjugated secondary Abs (Alexa Fluor 488/568/647, Abcam) at room temperature for 1 hour. Following incubations, the slides were washed twice with PBS-FSG-Tx100 for ten minutes. Upon completion of immunofluorescence staining, the sections were mounted with ProLong® Gold antifade reagent with DAPI (4′,6-diamidino-2-phenylindole) (Life Technologies) as a nuclear counterstain and coverslipped. Images were captured using a Leica SP8 confocal microscope.

RESULTS

Clinical assessment of rhesus macaques challenged with a Brazilian ZIKV isolate

In order to study ZIKV pathogenicity, immune responses and potential clinical symptoms, we inoculated a relatively high dose (10^7 PFUs) of a Brazilian viral strain (HS-2015-BA-01: GenBank Accession Number - KX520666.1, www.ncbi.nlm.nih.gov/genbank) i.v., similar to our dengue infection model (34) in 4 male Indian rhesus macaques. Multiple samples/tissues, including peripheral blood, saliva, urine, semen, LN biopsies and BM aspirates were collected at different time points (Figure 1A) to monitor viral and immune response dynamics. In spite of the high-dose inoculum, clinical or neurologic symptoms were never detected during the whole period of study and body weights remained stable (data not shown). Hematology and serum chemistry profiles showed individual fluctuations but no clear trend (Supplementary Figure 1).

ZIKV loads detection in blood and other body fluids

Plasma viral loads were positive already on day 1 post infection in 3 of 4 animals (00-R027, A7R014 and A7R078) peaking on day 3–4 with an average 23,379 copies/mL of plasma (10,870 to 74,945 copies/mL, Figure 1B). However, plasma viremia was rapidly resolved and became undetectable at 5–10 days post infection. In fact, only monkey A7L045 exhibited positive viremia from day 5 to 7. Although ZIKV has been reported to be detectable in semen and urine long after clearance of viremia, this was not the case here.

ZIKV RNA was found in semen and urine samples until day 7 and 14 respectively (Figures 1C–D). In fact, ZIKV RNA was detectable for extended periods of time in saliva samples (Figure 1E). Aside from plasma samples, ZIKV detection ranged between 70 to 2,200 copies/mL in the other body fluids.

ZIKV-eliciting antibody-secreting cell response and rapid GC formation

The kinetics of various B cell subsets were assessed post-infection including total, memory B cells and ASCs. Total B cells ($CD3^-/CD20^+$) numbers increased only on day 3. Within total B cells, activated ($CD3^-/CD20^+/HLADR^+/CD21^-/CD27^+$ (35)) and resting ($CD3^-/CD20^+/HLADR^+/CD21^+/CD27^+$ (35)) memory B cell numbers remained constant until day 70. The overall plasmablast ($CD3^-/CD20^-/CD14^-/CD16^-/CD11c^-/CD123^-/HLADR^+/CD80^+$ (32)) frequencies in blood, representative of an acute response peaked on day 5 post infection and again on day 42 (Figure 2A). The early plasmablast kinetic contrasts with those reported for infection of monkeys with an Asian (18) or African (17) ZIKV strains, which showed peak responses on days 7 or 10 respectively. The origin of the late plasmablast peak was not fully identified. However, ZIKV positive viral loads were detected in saliva samples from animals A7R014 and 00-R027, on day 42 (160 and 270 copies/mL respectively), suggesting that the second plasmablast response was also ZIKV-related. In an attempt to estimate ASC and antibody specificities, ZIKV NS1 and EDIII recombinant proteins were assayed by ELISPOT and ELISA respectively. Although the Env protein was available only for later time point analyses by ELISPOT, ZIKV NS1- and EDIII-specific ASCs could be enumerated from the LNs, BM and spleen within a month after infection (Figures 2B–C) and at day 142 (Figure 3E), but not from the peripheral blood (data not shown). However, on average, less than 50 NS1-specific IgG-, IgA- and IgM ASCs were detected per million LN and BM cells respectively (Figures 2B–C), which is considerably lower than the values obtained post simian immunodeficiency virus infection (144 and 1102 IgG ASCs in the blood and LNs respectively (Silveira, unpublished data)). Percentages of antigen-specific ASCs relative to total ASCs in LNs represented, on average, 1.74%, 4.9% and 1.3% of IgG, IgA and IgM-secreting cells respectively at day 14. BM ASCs detected on day 28 represented, on average, 0.64%, 0.3% and 0.35% of IgG+, IgA+ and IgM+ ASCs respectively. NS1-specific ASC frequency was maintained in similar values at day 142 in the axillary LNs, BM and spleen (Figure 3E). ZIKV NS1-specific IgG titers became detectable by day 28 in serum samples from 2 of 4 monkeys and increased, on average, almost 2-fold until day 70. Nevertheless, EDIII-specific IgG titers became detectable only by day 56 and remained stable until day 70 (Figure 2D). In this case, the detection of EDIII-specific antibodies may be a consequence of B cell restimulation since ZIKV loads were still found in saliva samples (Figure 1E) from some animals by day 42.

Since ZIKV-specific ASC and antibody responses were detected, we investigated their potential origin by evaluating the kinetics of germinal center (GCs) formation in LNs. GCs are characterized by the presence of proliferative B cells ($CD3^-/CD20^-/Ki67^+$), as the source of newly minted plasmablasts (32), and T follicular helper (Tfh) cells ($CD3^+/CD20^-/PD1^{hi}/CXCR5^+$) (36–38). The numbers of proliferating B cells were found to increase from day 7 to 14 (Figure 3A), leading to the rapid formation of B cell follicles (Figure 3B). Simultaneously, higher numbers of $CD4^+$ and $CD8^+$ PD-1^{hi} Tfh cells (39) were

observed (Figure 3C) in close proximity to the B cell follicle areas (data not shown), occupying relatively larger areas within the LNs (Figure 3D).

ZIKV alters the frequency of monocytes subsets and myeloid dendritic cells

Recently, CD14+/CD16+ monocytes were shown to elicit B cell differentiation into ASCs in the context of Dengue virus (DENV) infection *in vitro* (40). Thus, 3 monocyte populations ($CD14^+/CD16^+$, $CD14^+/CD16^-$ and $CD14^-/CD16^+$) were assessed in peripheral blood by flow cytometry. Percentages of $CD14^+/CD16^+$ cells increased almost 3-fold on days 2 to 5, in comparison to baseline levels. On the other hand, $CD14^+/CD16^-$ cells displayed increased cell frequencies on day 1, followed by much variation and a drop on day 28, to about half the baseline numbers. Only by day 70 post-infection these cells did return to their baseline frequencies. Of note, $CD14^-/CD16^+$ cells presented only a 3-fold percentage increase in frequency between days 28 and 42 (Figure 4A).

Both myeloid and plasmacytoid DC subsets were investigated. Total myeloid $CD16^-$ DCs (mDCs) exhibited a temporary decrease in frequency only on day 2, represented mainly by $CD11c^{hi}$ cells that almost disappeared from peripheral blood (Figure 4B). The frequencies of $CD16^+$ or $CADM1^+$ myeloid DCs were also assessed. Whereas $CD16^+/CD11c^{hi}$ mDC numbers had a continuous drop from day 10 to 42 after major fluctuations, $CD16^+/CD11c^{int}$ mDCs displayed increased frequencies from day 3 to 10, followed by a persistent marked reduction. A distinct DC subset ($CD11c^-/CD123^-/CADM1^+$), described in macaques as equivalent to murine $CD8a^+$ cells, sheep $CD26^+$ DCs and human $CD141^+$ cells (reviewed by (41)(41)) showed increased frequencies on days 3, 5, 21, 42 and 70 in comparison to baseline numbers (Figure 4C). Plasmacytoid DC (pDCs) numbers increased appreciably after day 10 (Figure 4B).

Absolute numbers of both monocyte and DC subsets varied only slightly up to day 28 (last time point for CBC data) (Supplemental Figures 2A–B), suggesting that the kinetics for the various subset based on relative values (percentage) reflected true changes induce by ZIKV infection.

Limited ZIKV effect on NK and total T cells

Since NK cells ($CD3^-/NKG2A^+/CD8^+/HLADR^-$) represent one of the initial anti-viral mechanisms, we evaluated the kinetics of 3 distinct subsets ($CD16^-/CD56^+$, $CD16^+/CD56^-$ and $CD16^+/CD56^+$) after infection. However, no major changes were seen for any subset (Figure 5A). A modest decrease in Perforin+/IFNγ- cell numbers within the $CD16^-/CD56^+$ subset from day 1 to 10 (Figures 5B–C) and a transient increase in perforin expression on $CD16^+/CD56^-$ cells were detected on day 14 (Figure 5D).

In contrast, variations in the subsets of CD4+ and CD8+ T cell frequencies were limited, with exception of naive and memory cells showing opposite transient trends on day 7 (Supplemental Figure 3A). Activated ($HLA\text{-}DR^+$) memory and effector CD4+ T cells presented marginal, but persistent increases in frequencies from days 3 and 5 on respectively (Supplemental Figures 3B–C). Proliferating ($Ki67^+$) $CD4^+$ T cells tended to decrease overtime though (Supplemental Figures 3D–E). For CD8+ T cell frequencies, all subsets remained stable throughout the study (Supplemental Figure 4A). Activated and proliferating

CD8+ T cells exhibited marginal changes with inverse patterns in comparison to their CD4+ counterparts (Supplemental Figures 4B–E).

DISCUSSION

Rhesus and cynomolgus macaques have been used to study ZIKV pathogenesis induced by this flavivirus infection. Distinct ZIKV isolates, such as African, Asian and South/Central American, have been chosen for animal challenges. As a standard pattern, viral RNA copies have been detected in plasma until day 7 to 14 upon viral challenges (16–18, 25, 30). Although transient viremia spikes were occasionally detected up to day 30 of infection in macaque plasma (22), ZIKV detection in fluids, such as urine or semen, has been negative after that period, in contrast to humans for which ZIKV persisted in these 2 compartments beyond plasma viremia. In fact, our data suggest that saliva may be an important site for longer maintenance of ZIKV particles in macaques. As hypothesized, the relatively high ZIKV inoculum delivered intravenously appeared to result in a faster viremia kinetic, but also resulted in earlier viral clearance from the blood (16, 18), in spite of a viral inoculum 10 times higher than any previously administered to rhesus macaques (16–18, 25, 30). The short viremia observed may also be secondary to the fact that the virus was a primary clinical isolate. It remains to be determined whether the route of infection and inoculum size (challenge dose) influence the magnitude and kinetics of viral replication in the host.

Besides viral loads, we and others showed that ZIKV infection can modulate the relative frequencies of several immune cell subsets (16–18), though variations may be more pronounced in lymphoid organs than in blood. Among B cells, we determined an earlier and a later plasmablast peak for a Brazilian ZIKV strain (Figure 2A) than for African and Asian strains (17, 18) which may be linked to the viral kinetics (Figure 1). However, plasmablast specificity has not been explored upon ZIKV infection yet. It is well known that DENV infection induces a robust, but transient plasmablast response in humans. Moreover, the majority of those plasmablasts are Env-specific and represent more than 50% of all circulating B cells post acute infection (42, 43). Nonetheless, DENV2 infection in monkeys leads to markedly higher viral loads than those observed in the current study (34). However, a direct comparison of plasmablasts from both infections was not possible as the procurement of ZIKV Env was delayed and evaluations of these responses were delayed in our ZIKV study. Conversely, NS1-specific ASCs were not tested in the context of our DENV infections and it is possible that that blood DENV NS1-specific ASCs frequencies be also low to undetectable during that infection. The low percentages of NS1-specific ASCs detected in tissues, such as LN, BM and spleen, suggest that ZIKV NS1 is probably not the most immunogenic antigen for antibody responses. ZIKV NS1-specific ASCs may also be mostly short-lived, which would impact their frequencies. Another potential explanation for the low responses may be the existence of inhibitory mechanisms induced by ZIKV infection. The expression of TACI and BCMA proteins, BAFF and APRIL receptors, have been demonstrated to be critical for the maintenance of ASC and antibody responses (44, 45). RNA-seq data from ZIKV infected neural progenitor cells showed downregulation of TNFRSF13C, another BAFF receptor (46). Considering that ZIKV loads can present a long duration in body fluids and antigen-specific ASCs are still found in low frequencies, it

remains to be elucidated whether ZIKV infection also dampens the expression of BAFF receptors in B cells *in vivo*, impacting the titers of anti-ZIKV antibodies.

Although marked GC formation was noted in LNs at day 14 after viral challenge (Figure 3), the antigen probably does not persist long enough, creating an asynchronous B cell selection that limits the magnitudes of ZIKV specific-ASC and antibody responses. DENV proteins and ZIKV RNA have been found in LNs at early time points after infection (16, 18, 47) concomitantly with GC B cells (47). To the best of our knowledge, our data represents the first description of GC cellular responses for ZIKV infection (Figure 3).

Recently, a monocyte subset ($CD14^{+}/CD16^{+}$) was described as able to elicit B cell differentiation into ASCs *in vitro* in the context of DENV infection (40). Although ZIKV infection increased the frequency of those cells from day 2 to 5 (Figure 4A), though this increase did not correlate with prominent ZIKV-specific ASC response (Figures 2B–C).

Although DCs have been also been reported as ZIKV permissive cells (15, 48, 49), the infection mainly affected $CD11c^{hi}$ mDCs in vivo (Figure 4B). Among receptors that mediate ZIKV cell entry, DC-SIGN is expressed only in mDCs (reviewed by (50)). pDCs on the other hand secrete high amounts of type I IFN after sensing virus entry reviewed by (51), which inhibits viral replication (15). Recently, pDC-derived type I IFN has been associated with expansion of B regulatory cells (Bregs) (52). Whether Bregs are generated during ZIKV infection *in vivo*, restricting antigen-specific antibody responses, remains to be investigated.

NK cells have been mainly associated with anti-viral responses through perforin and granzyme secretion to eliminate infected cells. In ZIKV challenged macaques, the frequency of activated (Ki67+) NK cells were reported as increased during peak viremia (16–18). However, we found no significant change in the kinetics of 3 distinct NK cell subsets in our study (Figure 5).

Blood T cell subsets, (naive and memory) showed surprisingly little variation post infection though increased levels of proliferation suggesting a moderate, but active response corroborating previous reports (17, 18). As a matter of fact, ZIKV Capsid and Env-specific cytokine-secreting T cells would represent less than 1% of all T cells (16). This could be secondary to the choice of antigen, as data from DENV infected patients point out that non-structural proteins contain more immunodominant T cell epitopes than structural proteins (reviewed in (53)).

In summary, our ZIKV animal model shows good evidence of virus infection and replication with a Brazilian ZIKV isolate, and the rapid viral kinetics concur with previous reports (16–18). The detailed analysis of multiple immune cell lineages, should contribute to the definition of immune correlates and the model provide a tool for testing the efficacy of vaccines and therapeutics against this viral infection.

Supplementary Material

Refer to Web version on PubMed Central for supplementary material.

Acknowledgments

The authors are indebted to the New Iberia Research Center (NIRC) veterinary and Research Resource personnel for providing excellent technical assistance. Also, we thank Dr. Luis C. S. Ferreira (The Vaccine Development Laboratory at the University of São Paulo, Brazil) for providing ZIKV-derived recombinant proteins and Dr. Chunxia Zhao (CDC, USA) for expert assistance with ELISPOT images.

This work was supported by part by grants 8R24OD010947 to FV and R01AI113883 and Nebraska Neuroscience Alliance Endowed Fund Award to SNB. The work at MMT lab received financial support from the Conselho Nacional de Pesquisa (CNPq, Brazil), Fundacao do Amparo a pesquisas do Estado de Minas Gerais (FAPEMIG, Brazil) and Conselho de Aperfeicoamento de Pessoal Nivel Superior (CAPES).

References

1. Foy BD, Kobylinski KC, Chilson Foy JL, Blitvich BJ, Travassos da Rosa A, Haddow AD, Lanciotti RS, Tesh RB. Probable non-vector-borne transmission of Zika virus, Colorado, USA. Emerg Infect Dis. 2011; 17:880–882. [PubMed: 21529401]
2. Musso D, Roche C, Robin E, Nhan T, Teissier A, Cao-Lormeau VM. Potential sexual transmission of Zika virus. Emerg Infect Dis. 2015; 21:359–361. doi: 310.3201/eid2102.141363. [PubMed: 25625872]
3. McCarthy M. Zika virus was transmitted by sexual contact in Texas, health officials report. BMJ. 2016; 352:i720.doi: 10.1136/bmj.i1720 [PubMed: 26848011]
4. Hayes EB. Zika virus outside Africa. Emerg Infect Dis. 2009; 15:1347–1350. doi: 1310.3201/eid1509.090442. [PubMed: 19788800]
5. Hazin AN, Poretti A, Di Cavalcanti Souza Cruz D, Tenorio M, van der Linden A, Pena LJ, Brito C, Gil LH, de Barros Miranda-Filho D, Marques ET, Turchi Martelli CM, Alves JG, Huisman TA. Computed Tomographic Findings in Microcephaly Associated with Zika Virus. N Engl J Med. 2016; 374:2193–2195. doi: 2110.1056/NEJMc1603617. Epub 1602016 Apr 1603616.
6. Mlakar J, Korva M, Tul N, Popovic M, Poljsak-Prijatelj M, Mraz J, Kolenc M, Resman Rus K, Vesnaver Vipotnik T, Fabjan Vodusek V, Vizjak A, Pizem J, Petrovec M, Avsic Zupanc T. Zika Virus Associated with Microcephaly. N Engl J Med. 2016; 374:951–958. [PubMed: 26862926]
7. van der Linden V, Filho EL, Lins OG, van der Linden A, Aragao Mde F, Brainer-Lima AM, Cruz DD, Rocha MA, Sobral da Silva PF, Carvalho MD, do Amaral FJ, Gomes JA, Ribeiro de Medeiros IC, Ventura CV, Ramos RC. Congenital Zika syndrome with arthrogryposis: retrospective case series study. BMJ. 2016; 354:i3899. [PubMed: 27509902]
8. Cao-Lormeau VM, Blake A, Mons S, Lastere S, Roche C, Vanhomwegen J, Dub T, Baudouin L, Teissier A, Larre P, Vial AL, Decam C, Choumet V, Halstead SK, Willison HJ, Musset L, Manuguerra JC, Despres P, Fournier E, Mallet HP, Musso D, Fontanet A, Neil J, Ghawche F. Guillain-Barre Syndrome outbreak associated with Zika virus infection in French Polynesia: a case-control study. Lancet. 2016; 387:1531–1539. doi: 1510.1016/S0140-6736(1516)00562-00566. Epub 02016 Mar 00562. [PubMed: 26948433]
9. Ventura CV, Maia M, Bravo-Filho V, Gois AL, Belfort R Jr. Zika virus in Brazil and macular atrophy in a child with microcephaly. Lancet. 2016; 387:228.
10. Wong G, Li S, Liu L, Liu Y, Bi Y. Zika virus in the testes: should we be worried? Protein Cell. 2017; 8:162–164. [PubMed: 28110372]
11. Cordeiro MT, Pena LJ, Brito CA, Gil LH, Marques ET. Positive IgM for Zika virus in the cerebrospinal fluid of 30 neonates with microcephaly in Brazil. Lancet. 2016; 387:1811–1812.
12. Faye O, Faye O, Diallo D, Diallo M, Weidmann M, Sall AA. Quantitative real-time PCR detection of Zika virus and evaluation with field-caught mosquitoes. Virol J. 2013; 10:311. [PubMed: 24148652]
13. Lanciotti RS, Kosoy OL, Laven JJ, Velez JO, Lambert AJ, Johnson AJ, Stanfield SM, Duffy MR. Genetic and serologic properties of Zika virus associated with an epidemic, Yap State, Micronesia, 2007. Emerg Infect Dis. 2008; 14:1232–1239. [PubMed: 18680646]

14. El Costa H, Gouilly J, Mansuy JM, Chen Q, Levy C, Cartron G, Veas F, Al-Daccak R, Izopet J, Jabrane-Ferrat N. ZIKA virus reveals broad tissue and cell tropism during the first trimester of pregnancy. Sci Rep. 2016; 6:35296. [PubMed: 27759009]
15. Hamel R, Dejarnac O, Wichit S, Ekchariyawat P, Neyret A, Luplertlop N, Perera-Lecoin M, Surasombatpattana P, Talignani L, Thomas F, Cao-Lormeau VM, Choumet V, Briant L, Despres P, Amara A, Yssel H, Misse D. Biology of Zika Virus Infection in Human Skin Cells. J Virol. 2015; 89:8880–8896. [PubMed: 26085147]
16. Osuna CE, Lim SY, Deleage C, Griffin BD, Stein D, Schroeder LT, Omange R, Best K, Luo M, Hraber PT, Andersen-Elyard H, Ojeda EF, Huang S, Vanlandingham DL, Higgs S, Perelson AS, Estes JD, Safronetz D, Lewis MG, Whitney JB. Zika viral dynamics and shedding in rhesus and cynomolgus macaques. Nat Med. 2016; 22:1448–1455. [PubMed: 27694931]
17. Aliota MT, Dudley DM, Newman CM, Mohr EL, Gellerup DD, Breitbach ME, Buechler CR, Rasheed MN, Mohns MS, Weiler AM, Barry GL, Weisgrau KL, Eudailey JA, Rakasz EG, Vosler LJ, Post J, Capuano S 3rd, Golos TG, Permar SR, Osorio JE, Friedrich TC, O'Connor SL, O'Connor DH. Heterologous Protection against Asian Zika Virus Challenge in Rhesus Macaques. PLoS Negl Trop Dis. 2016; 10:e0005168. [PubMed: 27911897]
18. Dudley DM, Aliota MT, Mohr EL, Weiler AM, Lehrer-Brey G, Weisgrau KL, Mohns MS, Breitbach ME, Rasheed MN, Newman CM, Gellerup DD, Moncla LH, Post J, Schultz-Darken N, Schotzko ML, Hayes JM, Eudailey JA, Moody MA, Permar SR, O'Connor SL, Rakasz EG, Simmons HA, Capuano S, Golos TG, Osorio JE, Friedrich TC, O'Connor DH. A rhesus macaque model of Asian-lineage Zika virus infection. Nat Commun. 2016; 7:12204. [PubMed: 27352279]
19. Govero J, Esakky P, Scheaffer SM, Fernandez E, Drury A, Platt DJ, Gorman MJ, Richner JM, Caine EA, Salazar V, Moley KH, Diamond MS. Zika virus infection damages the testes in mice. Nature. 2016; 540:438–442. [PubMed: 27798603]
20. Lazear HM, Govero J, Smith AM, Platt DJ, Fernandez E, Miner JJ, Diamond MS. A Mouse Model of Zika Virus Pathogenesis. Cell Host Microbe. 2016; 19:720–730. [PubMed: 27066744]
21. Ma W, Li S, Ma S, Jia L, Zhang F, Zhang Y, Zhang J, Wong G, Zhang S, Lu X, Liu M, Yan J, Li W, Qin C, Han D, Qin C, Wang N, Li X, Gao GF. Zika Virus Causes Testis Damage and Leads to Male Infertility in Mice. Cell. 2016; 167:1511–1524 e1510. [PubMed: 27884405]
22. Koide F, Goebel S, Snyder B, Walters KB, Gast A, Hagelin K, Kalkeri R, Rayner J. Development of a Zika Virus Infection Model in Cynomolgus Macaques. Front Microbiol. 2016; 7:2028. [PubMed: 28066354]
23. Cugola FR, Fernandes IR, Russo FB, Freitas BC, Dias JL, Guimaraes KP, Benazzato C, Almeida N, Pignatari GC, Romero S, Polonio CM, Cunha I, Freitas CL, Brandao WN, Rossato C, Andrade DG, Faria Dde P, Garcez AT, Buchpigel CA, Braconi CT, Mendes E, Sall AA, Zanotto PM, Peron JP, Muotri AR, Beltrao-Braga PC. The Brazilian Zika virus strain causes birth defects in experimental models. Nature. 2016; 534:267–271. [PubMed: 27279226]
24. Enfissi A, Codrington J, Roosblad J, Kazanji M, Rousset D. Zika virus genome from the Americas. Lancet. 2016; 387:227–228. [PubMed: 26775124]
25. Abbink P, Larocca RA, De La Barrera RA, Bricault CA, Moseley ET, Boyd M, Kirilova M, Li Z, Ng'ang'a D, Nanayakkara O, Nityanandam R, Mercado NB, Borducchi EN, Agarwal A, Brinkman AL, Cabral C, Chandrashekar A, Giglio PB, Jetton D, Jimenez J, Lee BC, Mojta S, Molloy K, Shetty M, Neubauer GH, Stephenson KE, Peron JP, Zanotto PM, Misamore J, Finneyfrock B, Lewis MG, Alter G, Modjarrad K, Jarman RG, Eckels KH, Michael NL, Thomas SJ, Barouch DH. Protective efficacy of multiple vaccine platforms against Zika virus challenge in rhesus monkeys. Science. 2016; 353:1129–1132. [PubMed: 27492477]
26. Larocca RA, Abbink P, Peron JP, Zanotto PM, Iampietro MJ, Badamchi-Zadeh A, Boyd M, Ng'ang'a D, Kirilova M, Nityanandam R, Mercado NB, Li Z, Moseley ET, Bricault CA, Borducchi EN, Giglio PB, Jetton D, Neubauer G, Nkolola JP, Maxfield LF, De La Barrera RA, Jarman RG, Eckels KH, Michael NL, Thomas SJ, Barouch DH. Vaccine protection against Zika virus from Brazil. Nature. 2016; 536:474–478. [PubMed: 27355570]
27. Sapparapu G, Fernandez E, Kose N, Bin C, Fox JM, Bombardi RG, Zhao H, Nelson CA, Bryan AL, Barnes T, Davidson E, Mysorekar IU, Fremont DH, Doranz BJ, Diamond MS, Crowe JE. Neutralizing human antibodies prevent Zika virus replication and fetal disease in mice. Nature. 2016; 540:443–447. [PubMed: 27819683]

28. Pardi N, Hogan MJ, Pelc RS, Muramatsu H, Andersen H, DeMaso CR, Dowd KA, Sutherland LL, Scearce RM, Parks R, Wagner W, Granados A, Greenhouse J, Walker M, Willis E, Yu JS, McGee CE, Sempowski GD, Mui BL, Tam YK, Huang YJ, Vanlandingham D, Holmes VM, Balachandran H, Sahu S, Lifton M, Higgs S, Hensley SE, Madden TD, Hope MJ, Kariko K, Santra S, Graham BS, Lewis MG, Pierson TC, Haynes BF, Weissman D. Zika virus protection by a single low-dose nucleoside-modified mRNA vaccination. Nature. 2017; 543:248–251. [PubMed: 28151488]
29. Stettler K, Beltramello M, Espinosa DA, Graham V, Cassotta A, Bianchi S, Vanzetta F, Minola A, Jaconi S, Mele F, Foglierini M, Pedotti M, Simonelli L, Dowall S, Atkinson B, Percivalle E, Simmons CP, Varani L, Blum J, Baldanti F, Cameroni E, Hewson R, Harris E, Lanzavecchia A, Sallusto F, Corti D. Specificity, cross-reactivity, and function of antibodies elicited by Zika virus infection. Science. 2016; 353:823–826. [PubMed: 27417494]
30. Li XF, Dong HL, Huang XY, Qiu YF, Wang HJ, Deng YQ, Zhang NN, Ye Q, Zhao H, Liu ZY, Fan H, An XP, Sun SH, Gao B, Fa YZ, Tong YG, Zhang FC, Gao GF, Cao WC, Shi PY, Qin CF. Characterization of a 2016 Clinical Isolate of Zika Virus in Non-human Primates. EBioMedicine. 2016; 12:170–177. [PubMed: 27693104]
31. Kasturi SP, Kozlowski PA, Nakaya HI, Burger MC, Russo P, Pham M, Kovalenkov Y, Silveira EL, Havenar-Daughton C, Burton SL, Kilgore KM, Johnson MJ, Nabi R, Legere T, Sher ZJ, Chen X, Amara RR, Hunter E, Bosinger SE, Spearman P, Crotty S, Villinger F, Derdeyn CA, Wrammert J, Pulendran B. Adjuvanting a Simian Immunodeficiency Virus Vaccine with Toll-Like Receptor Ligands Encapsulated in Nanoparticles Induces Persistent Antibody Responses and Enhanced Protection in TRIM5alpha Restrictive Macaques. J Virol. 2017; 91
32. Silveira EL, Kasturi SP, Kovalenkov Y, Rasheed AU, Yeiser P, Jinnah ZS, Legere TH, Pulendran B, Villinger F, Wrammert J. Vaccine-induced plasmablast responses in rhesus macaques: phenotypic characterization and a source for generating antigen-specific monoclonal antibodies. J Immunol Methods. 2015; 416:69–83. [PubMed: 25445326]
33. Gumber S, Nusrat A, Villinger F. Immunohistological characterization of intercellular junction proteins in rhesus macaque intestine. Exp Toxicol Pathol. 2014; 66:437–444. [PubMed: 25153024]
34. Onlamoon N, Noisakran S, Hsiao HM, Duncan A, Villinger F, Ansari AA, Perng GC. Dengue virus-induced hemorrhage in a nonhuman primate model. Blood. 2010; 115:1823–1834. [PubMed: 20042723]
35. Titanji K, Velu V, Chennareddi L, Vijay-Kumar M, Gewirtz AT, Freeman GJ, Amara RR. Acute depletion of activated memory B cells involves the PD-1 pathway in rapidly progressing SIV-infected macaques. J Clin Invest. 2010; 120:3878–3890. [PubMed: 20972331]
36. Hong JJ, Amancha PK, Rogers K, Ansari AA, Villinger F. Spatial alterations between CD4(+) T follicular helper, B, and CD8(+) T cells during simian immunodeficiency virus infection: T/B cell homeostasis, activation, and potential mechanism for viral escape. J Immunol. 2012; 188:3247–3256. [PubMed: 22387550]
37. Onabajo OO, George J, Lewis MG, Mattapallil JJ. Rhesus macaque lymph node PD-1(hi)CD4+ T cells express high levels of CXCR5 and IL-21 and display a CCR7(lo)ICOS+Bcl6+ T-follicular helper (Tfh) cell phenotype. PLoS One. 2013; 8:e59758. [PubMed: 23527264]
38. Petrovas C, Yamamoto T, Gerner MY, Boswell KL, Wloka K, Smith EC, Ambrozak DR, Sandler NG, Timmer KJ, Sun X, Pan L, Poholek A, Rao SS, Brenchley JM, Alam SM, Tomaras GD, Roederer M, Douek DC, Seder RA, Germain RN, Haddad EK, Koup RA. CD4 T follicular helper cell dynamics during SIV infection. J Clin Invest. 2012; 122:3281–3294. [PubMed: 22922258]
39. Im SJ, Hashimoto M, Gerner MY, Lee J, Kissick HT, Burger MC, Shan Q, Hale JS, Lee J, Nasti TH, Sharpe AH, Freeman GJ, Germain RN, Nakaya HI, Xue HH, Ahmed R. Defining CD8+ T cells that provide the proliferative burst after PD-1 therapy. Nature. 2016; 537:417–421. [PubMed: 27501248]
40. Kwissa M, Nakaya HI, Onlamoon N, Wrammert J, Villinger F, Perng GC, Yoksan S, Pattanapanyasat K, Chokephaibulkit K, Ahmed R, Pulendran B. Dengue virus infection induces expansion of a CD14(+)CD16(+) monocyte population that stimulates plasmablast differentiation. Cell Host Microbe. 2014; 16:115–127. [PubMed: 24981333]
41. Fossum E, Grodeland G, Terhorst D, Tveita AA, Vikse E, Mjaaland S, Henri S, Malissen B, Bogen B. Vaccine molecules targeting Xcr1 on cross-presenting DCs induce protective CD8+ T-cell responses against influenza virus. Eur J Immunol. 2015; 45:624–635. [PubMed: 25410055]

42. Garcia-Bates TM, Cordeiro MT, Nascimento EJ, Smith AP, Soares de Melo KM, McBurney SP, Evans JD, Marques ET Jr, Barratt-Boyes SM. Association between magnitude of the virus-specific plasmablast response and disease severity in dengue patients. J Immunol. 2013; 190:80–87. [PubMed: 23203929]
43. Wrammert J, Onlamoon N, Akondy RS, Perng GC, Polsrila K, Chandele A, Kwissa M, Pulendran B, Wilson PC, Wittawatmongkol O, Yoksan S, Angkasekwinai N, Pattanapanyasat K, Chokephaibulkit K, Ahmed R. Rapid and massive virus-specific plasmablast responses during acute dengue virus infection in humans. J Virol. 2012; 86:2911–2918. [PubMed: 22238318]
44. O'Connor BP, Raman VS, Erickson LD, Cook WJ, Weaver LK, Ahonen C, Lin LL, Mantchev GT, Bram RJ, Noelle RJ. BCMA is essential for the survival of long-lived bone marrow plasma cells. J Exp Med. 2004; 199:91–98. [PubMed: 14707116]
45. Wolf AI, Mozdzanowska K, Quinn WJ 3rd, Metzgar M, Williams KL, Caton AJ, Meffre E, Bram RJ, Erickson LD, Allman D, Cancro MP, Erikson J. Protective antiviral antibody responses in a mouse model of influenza virus infection require TACI. J Clin Invest. 2011; 121:3954–3964. [PubMed: 21881204]
46. Ghouzzi VE, Bianchi FT, Molineris I, Mounce BC, Berto GE, Rak M, Lebon S, Aubry L, Tocco C, Gai M, Chiotto AM, Sgro F, Pallavicini G, Simon-Loriere E, Passemard S, Vignuzzi M, Gressens P, Di Cunto F. ZIKA virus elicits P53 activation and genotoxic stress in human neural progenitors similar to mutations involved in severe forms of genetic microcephaly and p53. Cell Death Dis. 2016; 7:e2440. [PubMed: 27787521]
47. Yam-Puc JC, Garcia-Cordero J, Calderon-Amador J, Donis-Maturano L, Cedillo-Barron L, Flores-Romo L. Germinal center reaction following cutaneous dengue virus infection in immune-competent mice. Front Immunol. 2015; 6:188. [PubMed: 25964784]
48. Jurado KA, Simoni MK, Tang Z, Uraki R, Hwang J, Householder S, Wu M, Lindenbach BD, Abrahams VM, Guller S, Fikrig E. Zika virus productively infects primary human placenta-specific macrophages. JCI Insight. 2016; 1
49. Quicke KM, Bowen JR, Johnson EL, McDonald CE, Ma H, O'Neal JT, Rajakumar A, Wrammert J, Rimawi BH, Pulendran B, Schinazi RF, Chakraborty R, Suthar MS. Zika Virus Infects Human Placental Macrophages. Cell Host Microbe. 2016; 20:83–90. [PubMed: 27247001]
50. van Kooyk Y, Geijtenbeek TB. DC-SIGN: escape mechanism for pathogens. Nat Rev Immunol. 2003; 3:697–709. [PubMed: 12949494]
51. Yockey LJ, Varela L, Rakib T, Khoury-Hanold W, Fink SL, Stutz B, Szigeti-Buck K, Van den Pol A, Lindenbach BD, Horvath TL, Iwasaki A. Vaginal Exposure to Zika Virus during Pregnancy Leads to Fetal Brain Infection. Cell. 2016; 166:1247–1256 e1244. [PubMed: 27565347]
52. Menon M, Blair PA, Isenberg DA, Mauri C. A Regulatory Feedback between Plasmacytoid Dendritic Cells and Regulatory B Cells Is Aberrant in Systemic Lupus Erythematosus. Immunity. 2016; 44:683–697. [PubMed: 26968426]
53. Rothman AL. Immunity to dengue virus: a tale of original antigenic sin and tropical cytokine storms. Nat Rev Immunol. 2011; 11:532–543. [PubMed: 21760609]

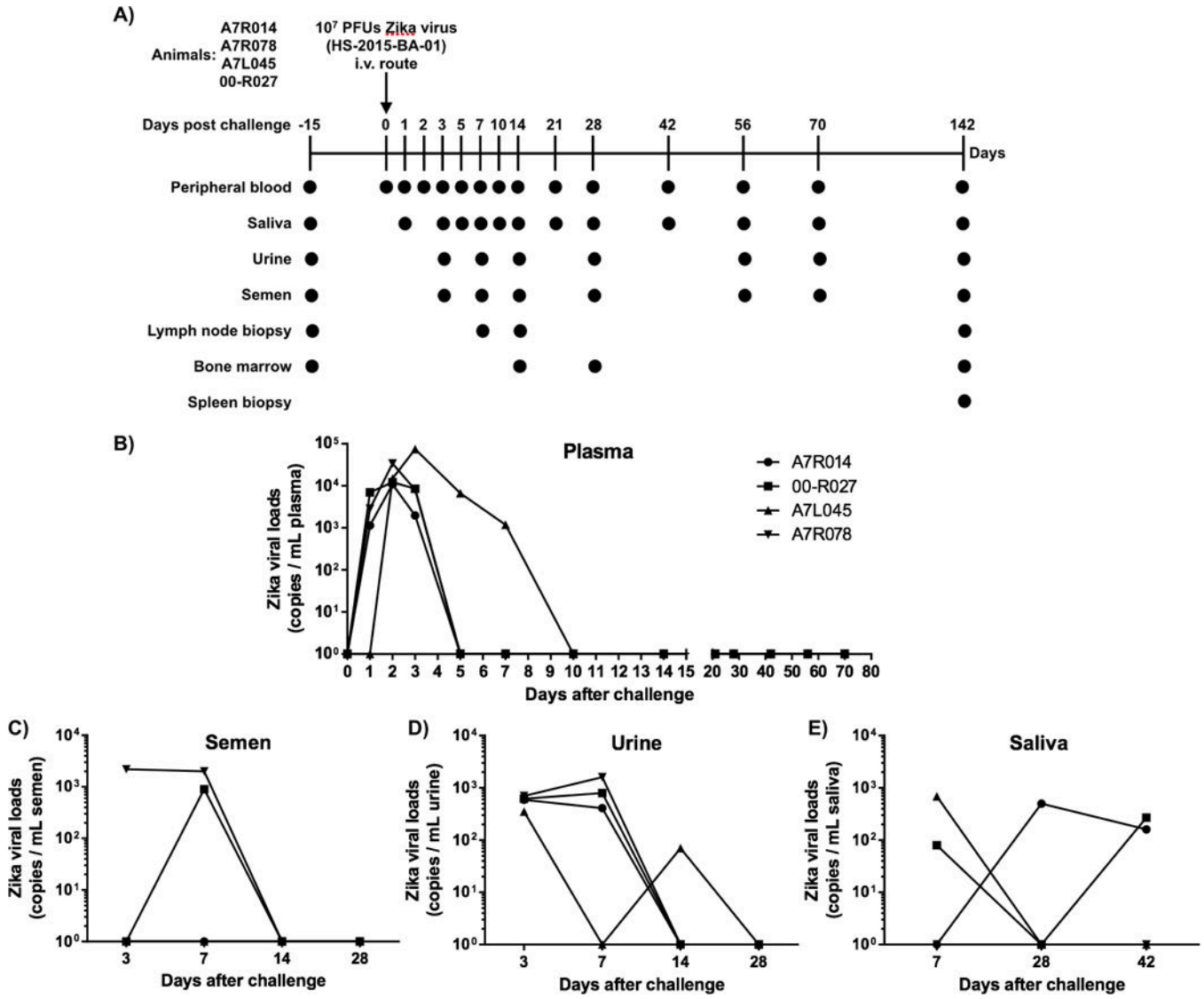

Figure 1.

Scheme of ZIKV virus challenge and tissue sampling and short ZIKV detection rhesus macaque plasma. A) 107 PFUs of ZIKV (HS-2015-BA-01 strain - GenBank Acession Number - KX520666.1) were administrated via intravenous route in 4 rhesus macaques. Multiple tissues and fluids were collected in indicated time points. B) Isolated plasma samples had their total RNA reverse-transcribed before performance of ZIKV-specific quantitative PCR assay at different time points.

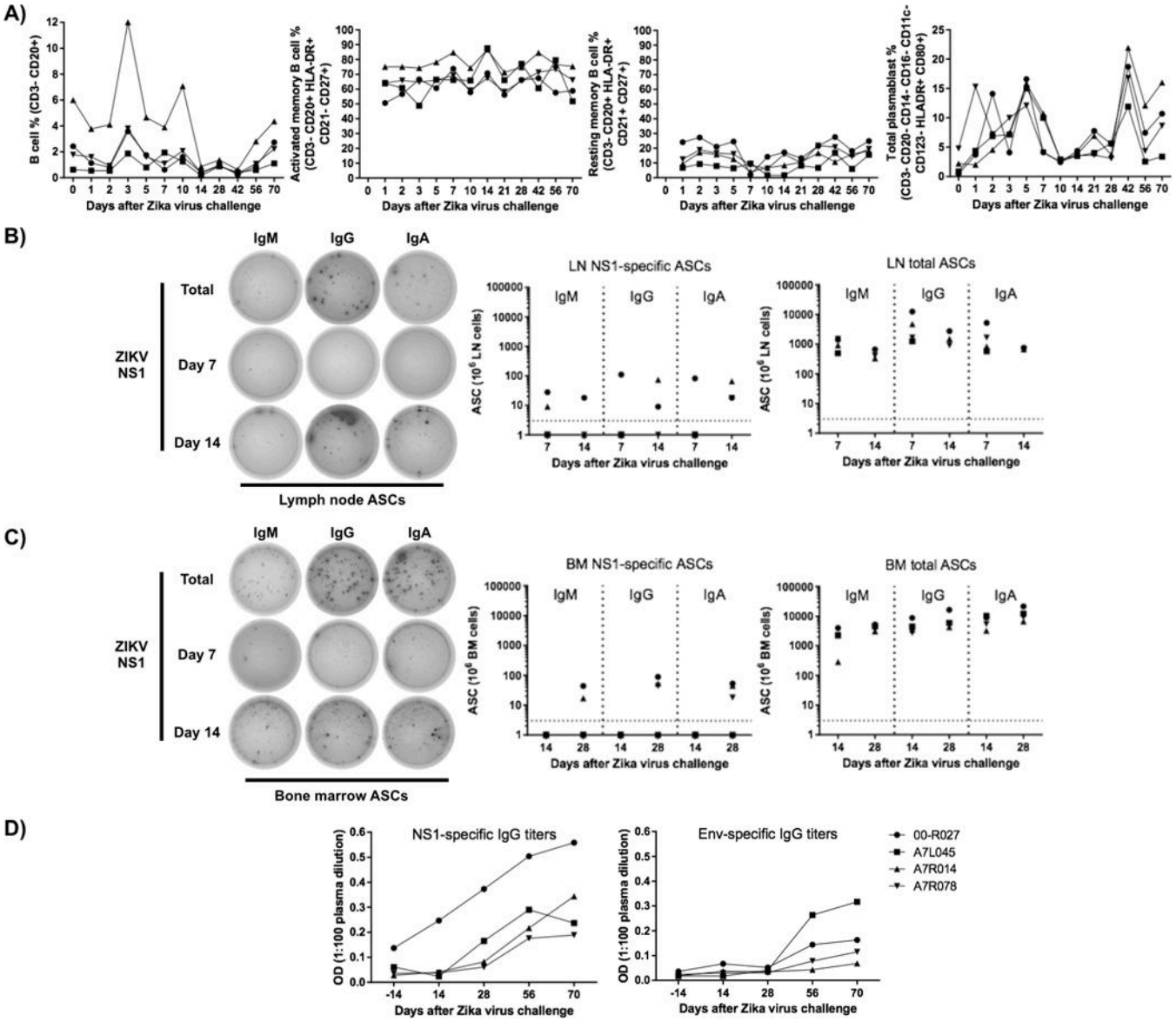

Figure 2.

Total B cells and plasmablasts (blood ASCs) have their frequency increased at early time points after ZIKV challenge with a Brazilian isolate in rhesus macaques. Analytical flow cytometry was performed in total, activated memory, resting memory B cells and total plasmablasts from PBMCs. The enumeration of ZIKV-specific antibody-secreting cells were done at different time points with LN (B) and BM cells (C) based on the recognition of NS1 recombinant protein by ELISPOT. NS1-specific LN wells shown in B (left) were plated with 1.08×10^5 cells, while total Ig wells had 0.12×10^5 cells respectively. BM wells shown in C (left) were plated with 1.125×10^5 cells for NS1 and 0.04×10^5 cells for total Ig wells. E) Representative images showing ASC quantification at day 142 after ZIKV infection, wells were plated with 1.08×10^5 cells for axillary LN cells, while total Ig wells from bone marrow and spleen received 0.36×10^5 cells.

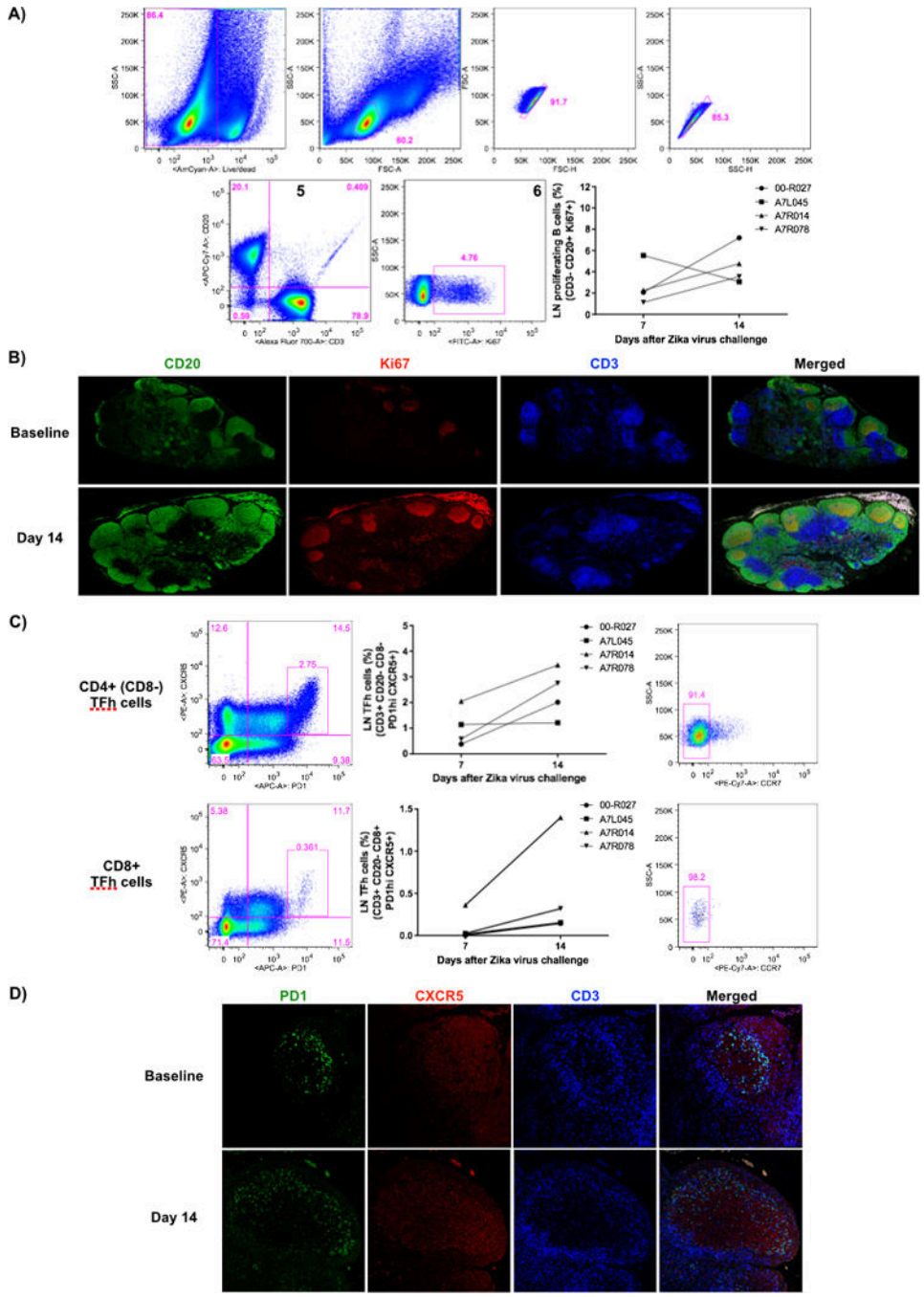

Figure 3.

Rapid germinal center (GC) reactions LNs after ZIKV challenge. A) Representative flow cytometry data showing a sequential gating strategy to enrich for proliferating B cells: 1) Live cells; 2) Lymphocytes; 3–4) Singlets; 5) $CD3^{-}/CD20^{+}$ cells; and 6) Ki67+ cells at days 7 and 14 after ZIKV challenge. Proliferating B cells ($CD3^{-}/CD20^{+}/Ki67^{+}$) and formation of B cell follicles presented increased frequency in the LNs at day 14 by flow cytometry (A) and tissue immunofluorescence (B). C) Representative flow cytometry data showing a Tfh cell gating. During formation of B cell follicles, increased frequency of CD4 and CD8 Tfh

cells ($CD3^+/CD20^-/CD8^{-/+}/PD1^{hi}/CXCR5^+/CCR7^-$) were detected in the LNs at day 14 of challenge by flow cytometry (C) and tissue immunofluorescence assays (D).

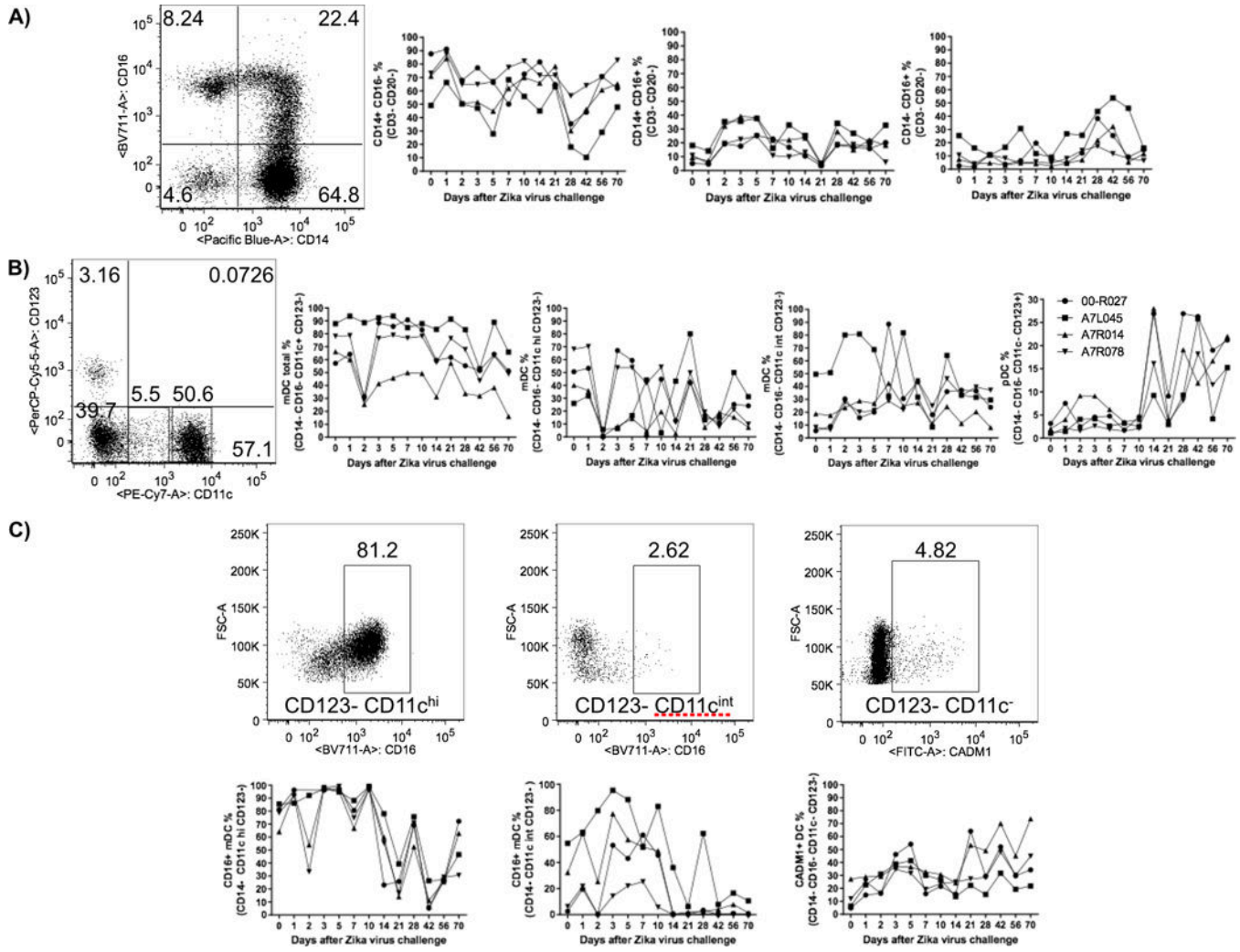

Figure 4.

ZIKV challenge presented differential impact over monocyte and DC subsets from rhesus macaque PBMC. A) After staining PBMCs for $CD14^{+}/CD16^{-}$ (left plot), $CD14^{+}/CD16^{+}$ (center plot) and $CD14^{+}/CD16^{+}$ (right plot) monocytes, their respective percentages were evaluated by flow cytometry at early time points after ZIKV challenge. A) Representative flow cytometry data showing a monocyte ($Live^{+}/CD3^{-}/CD20^{-}/HLA\text{-}DR^{+}$) gate based on CD14 and CD16 expressions (left plot). Whereas ZIKV infection does not change the cell frequencies of $CD14^{-}/CD16^{+}$ monocytes, there was an increase for $CD14^{+}/CD16^{+}$ cells from day 2 to 5 and a continuous decrease for $CD14^{+}/CD16^{-}$ monocytes from day 1 to day 28 upon viral challenge. B) Representative flow cytometry data showing a DC ($Live\ CD3^{-}/CD20^{-}/CD8^{-}/CD14^{-}/HLA\text{-}DR^{+}$) gate based on CD11c and CD123 expressions. The kinetics of different dendritic cell subsets, total myeloid, myeloid ($CD123^{-}/CD11c^{hi}$) and ($CD123^{-}/CD11c^{int}$) and plasmacytoid ($CD123^{+}/CD11c^{-}$) were assessed upon ZIKV challenge. Whereas ZIKV infection punctually decreased the total and $CD11c^{hi}$ mDC frequencies at day 2, the opposite was observed for pDCs after day 10. C) Representative flow cytometry data showing distinct myeloid DCs based on $CD16^{+}$ or $CADM1^{+}$ expression (upper plots) within the respective DC subsets, followed by their kinetics data (lower plots).

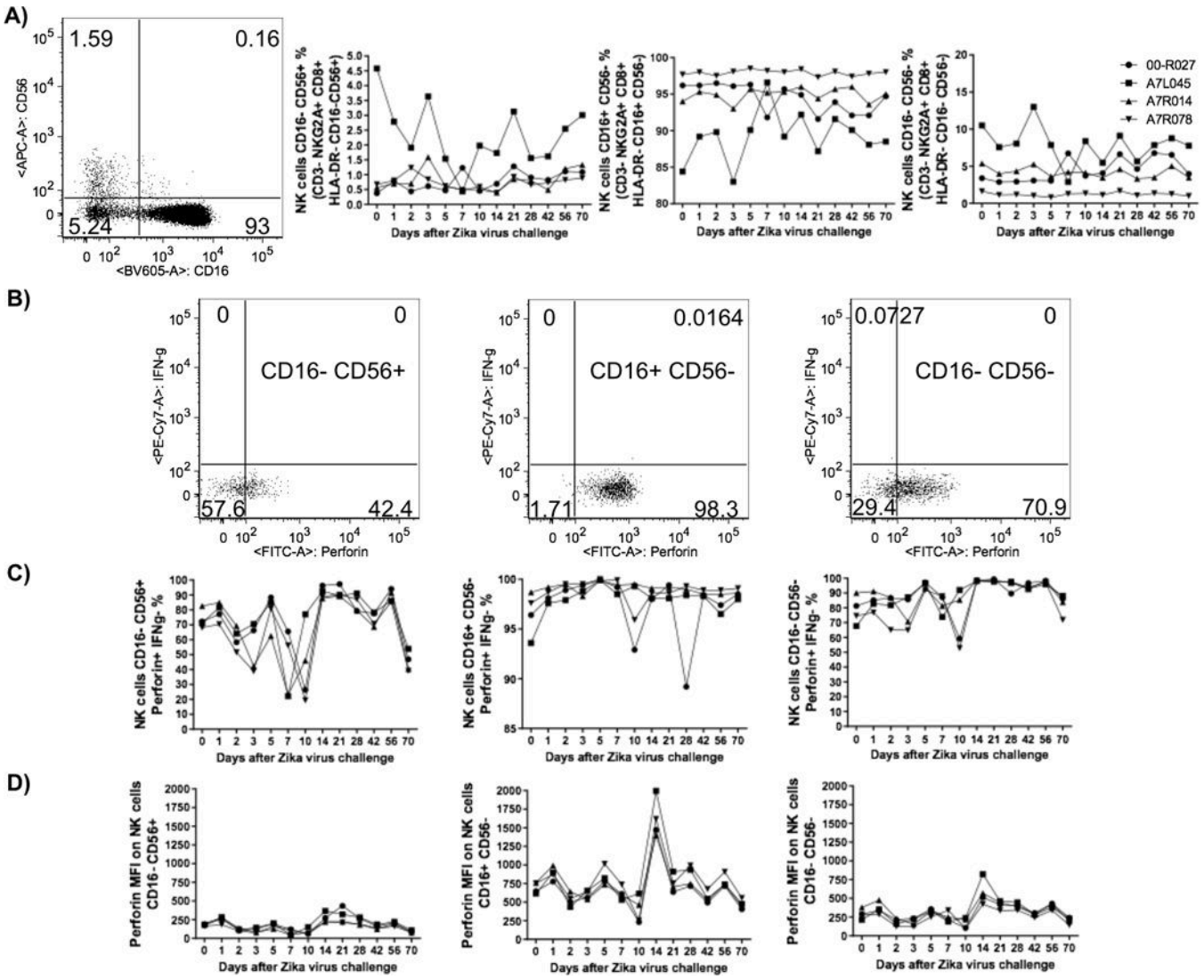

Figure 5.

ZIKV challenge had limited impact on the frequency of NK cell subsets and their functionality in rhesus macaque PBMC. A) Representative flow cytometry data (left plot) showing a NK cell ($CD3^-/NKG2A^+/CD8^+/HLA\text{-}DR^-$) gate based on CD16 and CD56 expression as well as their respective kinetics data for the following cell subsets $CD16^-/CD56^+$, $CD16^+/CD56^-$ and $CD16^-/CD56^-$. B) Representative flow cytometry data for Perforin and IFNγ-secreting NK cells and the kinetics data for $Perforin^+$ IFNγ^- NK cell subsets (C). The level of Perforin expression (MFI values) was measured within the distinct NK cell subsets (D).